06

Effect of Hydrogen on the Corrosion Resistance of Duplex Stainless Steel

© A.I. Petrov, M.V. Razuvaeva

Ioffe Institute,
194021 St. Petersburg, Russia
e-mail: An.Petrov@mail.ioffe.ru, M.Razuvaeva@mail.ioffe.ru

Received July 19, 2023
Revised September 15, 2023
Accepted September 15, 2023

The features of diffusion in two-phase (duplex) stainless steel (DSS), interaction the effect of hydrogen with trap sites in various steel structures, the influence of plastic deformation, local stresses and hydrogen concentrations on localized corrosion and hydrogen embrittlement. Available data indicate that the diffusivity of DSS is insensitive to plastic deformation and increase in dislocation density, but it is influenced by grain boundaries and interfaces α/γ-phases The influence of hydrogen on stability is considered γ-phases, formation of second phases and hydrogen trap semi-coherent grain boundaries. The mechanisms that ensure crack propagation are discussed: brittle, associated with decohesion in the region of maximum hydrostatic stress, and plastic in the austenite phase — due to shear decohesion along the slip plane. Reviewed the influence of the yield stress of duplex steel on the susceptibility to hydrogen embrittlement, as well as on correlation of the steel embrittlement index with the total amount of absorbed hydrogen.

Keywords: hydrogen embrittlement, duplex stainless steel, microstructure, hydrogen traps, diffusion, grain and phase boundaries.

DOI: 10.61011/TP.2023.11.57498.184-23

Introduction

Stress corrosion cracking (SCC) is a serious problem for oil and gas production, in particular, for deep-well drilling. Fluid in such wells contains a lot of salt water, H_2S and CO_2. Depending on temperature and composition, this corrosive environment may cause general corrosion, local corrosion and stress corrosion cracking of steels. One of the method for protection against such problems involves the use of duplex stainless steels (DSS) in such corrosive environment. DSS feature two-phase microstructure with almost equal ferrite (BCC, α) and austenite (FCC, γ) fractions. Microstructure of such steels usually consists of austenite grains elongated in rolling direction and located in the ferrite matrix. The length of cylindrical austenite grains is several times greater than their diameter.

Duplex stainless steels have advantageous combination of stress-strain properties, pitting corrosion resistance and stress corrosion cracking. In acid environments with H_2S, corrosion reactions result in formation of bivalent ferrous ions in anodic areas and hydrogen ion reduction in cathodic areas. The presence of H_2S suppresses hydrogen molization, thus, facilitating H atom penetration in steel and hydrogen embrittlement of the material. External factors (pressure, H_2S, chloride concentration, solution temperature, acidity pH of solution) and internal factors (alloy composition, heat and cold treatment, strength, surface condition) contribute to hydrogen embrittlement (HE). In addition, other contributing factors, besides those listed above, shall be considered for forecasting HE in DSS. These include local hydrogen concentration, stress distribution near the growing crack, hydrogen resistance of austenite, etc.

Data allowing the assessment of contribution made by some of the factors listed above to corrosion resistance and embrittlement of SAF2205 type duplex stainless steels is addressed herein.

1. Hydrogen interaction with structure defects

Steel susceptibility to hydrogen embrittlement is directly associated with hydrogen interaction with various structure defects that are hydrogen traps. Hydrogen trapping susceptibility is defined by the trap binding energy E_b [1]:

$$E_b = E_a - E_d, \tag{1}$$

where E_a is the activation energy of H release from the trap, E_d is the activation energy of H atom jump from the trap site to lattice sites. It is known [1,2] that traps with activation energies of $E_a \leq 60$ kJ/mol are characterized as reversible traps. Such traps affect considerably on the steel susceptibility to hydrogen embrittlement because they are the sources of H atoms. According to [3], reversible traps with energy up to 20 kJ/mol are assigned to elastic stress field; reversible traps with energy within (20–30) kJ/mol are assigned to grain boundaries; within (40 – 55) kJ/mol — to austenite-ferrite interfaces. Traps with energy of $E_a \geq 60$ kJ/mol are referred to as irreversible traps [4]. Such traps in DSS include, for example, ε-martensite or α-martensite phase. The role of irreversible H trap sites is to prevent hydrogen embrittlement.

2. Hydrogen effect on duplex steel structure and fracture

In [1], H interaction with various trap sites and hydrogen trapping in various DSS structures were investigated. Local stress effect on phase transitions and hydrogen cracking are also discussed. Hydrogen charging of steel was carried out at 18°C in H_2SO_4 aqueous solution at constant current density 500 A/m^2. H trapping mechanisms in DSS (SAF2205) were investigated using thermal desorption spectroscopy (TDS). It was found that hydrogen charging followed by sample holding during a month at room temperature resulted in formation of needle-shaped ε-martensite an heavy cracking on the sample surfaces. Similar data on DSS austenite transformation into ε-martensite was also obtained by other authors [5].

In [6], however, it is shown that even at plastic strain 17.5%, no ε-martensite is observed on the X-ray images of DSS samples. The difference may be possibly caused by different current density used for hydrogen charging: it is just 127 A/m^2 in [6] that could lead to reduction of hydrogen penetration flux into steel.

Most cracks occur inside theγ-phase or at the α/γ-phase interface. It is believed in [1] that cracking occurred due to high tensile stresses induced in the surface layer as a result of low hydrogen diffusion within the austenite phase. Actually, hydrogen that diffuses into steel dissolves differently in ferrite and austenite. H solubility in austenite is 2 to 3 orders of magnitude higher than in ferrite, while the hydrogen diffusion constant in ferrite is four to five orders of magnitude higher than in austenite [6,7].

Thus, hydrogen desorption after ageing of hydrated samples resulted in phase transition — formation of ε-martensite in the γ-phase. However, samples with high concentration of ε-martensite were found to have minimum surface cracking. Therefore, high stability of γ-phase results in lower concentration of ε-martensite phase and higher degree of fracture.

Investigation of hydrogen desorption allowed to identify H trap sites. These were reversible traps with activation energies of 20 kJ/mol and 34 kJ/mol and irreversible traps with energy of 62 kJ/mol. Irreversible H trapping was found to be associated with mass formation ($\sim$ 35% by weight) of ε-martensite phase.

It is suggested that susceptibility of duplex steel 2205 to hydrogen damage mechanism is defined by a microstructure that occurs in the γ-phase in interaction with hydrogen. Lower stability of the γ-phase causes higher concentration of ε-martensite and lower embrittlement.

The impact of second phases induced by hydrogen by two different DSS hydrogen-charging methods: with cathodic charging (at a current density of 500 A/m^2 in H_2SO_4 solution) and with gas charging at 60 MPa and 300°C was investigated in [8]. Activation energy of hydrogen release from trap during sample heating up to 500°C was also estimated. During cathodic charging, like in the previous study [6], occurrence of ε-martensite in the form of lath martensite was observed after long-term holding of the samples at room temperature. Lower hydrogen diffusion in the γ-phase is also a cause of ε-martensite occurrence. This causes high stresses in the γ-phase on the sample surface, where, as shown by the X-ray measurements, hydrogen increases the lattice constant. The TDS method showed that after cathodic charging during 24 h the hydrogen desorption activation energies were equal to 20 kJ/mol, 35 kJ/mol and 40 kJ/mol. An additional peak with energy $E_a = 63$ kJ/mol occurs in the sample after long-term cathodic charging during 72 h in the temperature range of 300$-$400°C. This irreversible H trapping peak was assigned to hydride phase γ^* that is a hydrogen-enriched austenite phase with lattice constant higher by 5%. The concentration of the γ^*-phase was estimated as 10% of the total sample.

After gas-phase charging under pressure, H desorption has its peak within 55$-$100°C with H release activation energy about 20 kJ/mol and the major peak in the temperature range of 340$-$390°C with $E_a = 70$ kJ/mol. This peak was assigned to the σ-phase of intermetallic Fe(CrMo) compound [2,4,8]. During following cooling to room temperature, the peak that had been detected after heating disappeared.

Thus, it was found that the secondary σ-phase and γ^* hydride occur in DSS at high heating temperatures depending on the charging conditions. The impact of irreversible trapping energy and second phase concentrations on DSS embrittlement are also discussed herein. Heavy surface cracking of the sample was detected in the cathode-charged samples. No cracking signs were detected in the samples charged under pressure. Cracking observed after cathodic charging was interpreted as hydrogen-induced cracking at the α/γ interfaces due to the hydrogen diffusion difference in both duplex steel phases.

3. Hydrogen interaction with phase and grain boundaries

As mentioned above, the investigation of hydrogen diffusion and interaction with traps is critical for understanding the DSS hydrogen embrittlement mechanism. It is reported that the role of hydrogen traps, in particular interphase boundaries, has been studied insufficiently. In [9], it is shown that the core dislocation at the ferrite$-$NbC interface acts as deep traps. The authors of [6] assumed that the similar trapping mechanism may be available at the semicoherent austenite$-$ferrite interfaces. To check this assumption, interaction with various structural defects induced by plastic strain of DSS was investigated.

Samples after tensile strain up to 4.6%, 8.6%, 17.5% were investigated. Hydrogen charging was carried out in 0.05 mol/l H_2SO_4 solution at a current density of 127 A/m^2. After hydrogen charging, the samples were placed in air for hydrogen release.

It is shown that the volume ratio of austenite (43%) remained unchanged suggesting the mechanical stability of

austenite. Moreover, X-ray measurements have shown that there was no ε-martensite. The hydrogen diffusion constant in steel was found to vary just slightly with growing strain and ρ_d dislocation density. With strain growing up to 17.5%, ρ_d is approximately 3 times as high, while the dislocation density in austenite was higher than in ferrite. It was suggested that diffusion capability of DSS 2205 was insensitive to plastic strain and increasing dislocation density, but was dependent on the ferrite grain boundaries and α/γ-phase interfaces.

It is known that local disorientation increases near grain boundaries with increasing strain. Herein, the average local disorientations increased from 0.1 to 0.3° with maximum increase in dislocation density .

To estimate hydrogen distribution in steel microstructure, a hydrogen microprint method was used that implied silver ion reduction from AgBr emulsion by hydrogen atoms. It is shown that dislocations have negligible effect on Ag particle segregation. At the same time, large and dense silver particles are observed at the ferrite phase and grain boundaries. Thus, the ferrite phase and grain boundaries are the main hydrogen traps in DSS.

The nature of H trap by these boundaries may be attributed to coherent interfaces, boundary dislocations or distorted interstitial. Atomic structure of mismatch dislocations and coherent area fraction of the austenite–ferrite interfaces depend on the disorientation angle to a great extent. The interface binding energy increases with decreasing interface coherency from$(15-30)$ kJ/mol for the coherent boundary up to $(36-71)$ kJ/mol for the semicoherent boundary [9,10]. The binding energy of the ferrite–austenite interface is within $(40-50)$ kJ/mol, and the average binding energy is 43.6 kJ/mol according to the estimate in [6].

In [6] it is pointed out that phase boundaries act not only as powerful hydrogen traps, but also make the H diffusion paths more tortuous due to diffusion energy barrier at the ferrite–austenite interface.

This barrier is associated with hydrogen atom jumping from the interface site to the austenite lattice site, and its estimated value is close to 100 kJ/mol.

4. Hydrogen effect on localized corrosion

Let's consider the features of the localized corrosion of duplex steel (DSS). First of all, it should be noted that due to their two-phase composition, these steels suffer selective corrosion (SD) that is commonly examined by anodic polarization test method.

Active corrosion of alloy 2205 in a highly acid solution containing HCl and H_2SO_4 with high chloride and sulfide concentrations within 25–60°C is described in [11] . The tests have shown that steel corrosion rate in such solution was particularly high — $17.57 \cdot 10^{-3}$ m/year. Increased Cr and Mo concentrations improve passivating power of duplex steel, while chloride addition degrades the passivating power. Two current density peaks are observed in transition from active to passive corrosion. Such peaks, according to [11,12], are caused by selective dissolution of the ferrite and austenite phases. It is pointed in [13] that selective dissolution is also initiated when external stress is absent at $\sigma = 0$, i.e. it depends on passive film instability. During SCC testing of duplex stainless steel, SD of one phase is observed in environment with high chloride concentrations, low pH, in presence of H_2S.

Ferrite serves as the corrosive phase most often, but in acid environments austenite dissolution is also possible [14]. According to [15], nitrogen content may affect considerably the behavior of primarily the corrosive phase. Thus, when nitrogen concentration in austenite is high, this phase is resistant to chlorine ions, therefore, when the chloride level is high, ferrite primarily suffers corrosion. On the contrary, when the chloride concentration is low, higher Cr and Mo doping of ferrite increases its corrosion resistance. In [16], it was found that relative nobility of each phase depends the test environment.

In [17], the potentiostatic polarization method was used to examine the elastic stress impact within 0.5–0.9 from the magnitude of σ_{02} and plastic strain (5, 10, 15%) on the resistance to uniform and pitting corrosion of DSS 2205 in 3.5% NaCl and 2 mol/l HCl solution. It is shown that the elastic stress has a negligible effect on the anodic current and corrosion current density within the passivation range.

The corrosion current density increases with increasing pre-strain level. Within the passivation range, the corrosion current density increases with potential displacement in positive direction in case of pre-strain, however, the pitting potential remains the same at different pre-strain levels. It is shown that elastic stresses and plastic pre-strain do not affect the uniform corrosion and pitting corrosion.

It has been also found that pitting corrosion of DSS is always localized in austenite grains, when the strain is lower than 5%. In case when the strain level is higher than 5%, pitting is localized at the intersection of ferrite and austenite grains.

Based on the duplex structure strain mechanism, DSS pitting corrosion behavior in plastic strain is explained in [17] as follows. According to [18], compressive microstresses occur in ferrite and balancing tensile microstresses occur in austenite during duplex steel heat treatment. Yield phenomenon takes place primarily in the austenite phase. When the strain is not higher than 5%, the austenite phase is tensile stressed that may explain pitting location in the austenite phase. Dislocation accumulation near the grain boundaries when the strain is higher than 5% results in high stress concentration and, therefore, to localized corrosion at the ferrite and austenite grain intersection.

As shown above, pre-strain of the DSS samples reduces the protective film stability resulting in pitting corrosion. This data suggests that plastic pre-strain may also affect considerably the hydrogen embrittlement susceptibility of duplex steel. For this purpose, let's consider the data

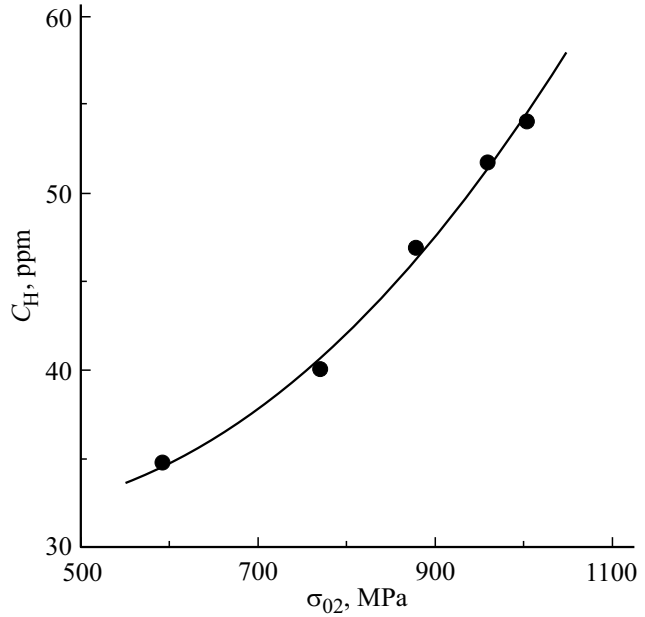

Figure 1. Hydrogen concentration dependence on yield stress of duplex steel 2205.

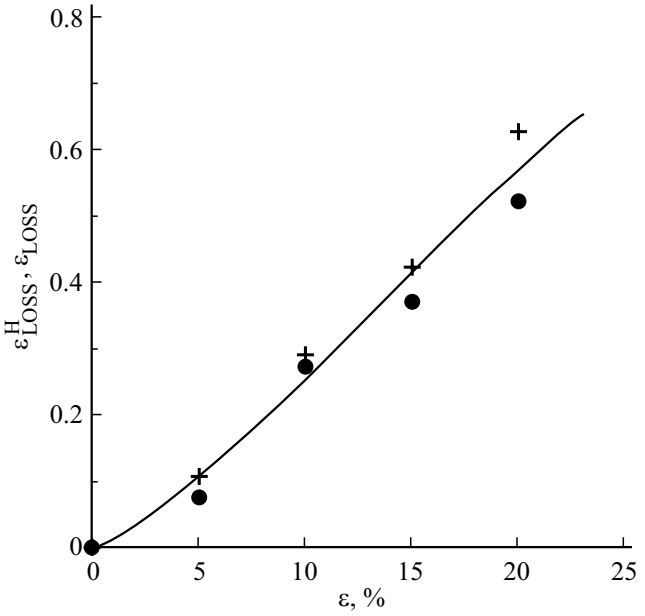

Figure 2. Dependence of loss of plasticity on pre-strain for DSS samples without hydrogen ε_{LOSS} (•) and after hydrogen saturation ε^H_{LOSS} (+).

in [19] regarding the impact of pre-strain and following cathodic charging of DSS samples on the SCC development susceptibility. Duplex steel 2205 samples with various degrees of strain within 0−20% were subjected to cathodic hydrogen charging in 0.5 mol/l H_2SO_4 solution at a current density of 100 A/m^2 during 48 h at18°C. Then the samples were immediately stressed to rupture at a constant strain rate of $2.7 \cdot 10^{-4}\,s^{-1}$ in room conditions. Pre-strained samples, but without hydrogen charging, were used as test samples.

Strength performance variation (σ_{02} and σ_B) of the initial strained samples, strain to rupture (ε_o), strain after hydrogen charging (ε^f_H) and loss of plasticity were estimated:

$$\varepsilon^H_{LOSS} = \frac{\varepsilon_0 - \varepsilon^f_H}{\varepsilon_0}. \quad (2)$$

For comparison, the loss of plasticity of pre-strained samples was estimated, but without hydrogen saturation:

$$\varepsilon_{LOSS} = \frac{\varepsilon_0 - \varepsilon^f}{\varepsilon_0}, \quad (3)$$

where ε^f is the strain to rupture.

It is shown that steel is strengthened considerably during pre-straining: thus, the yield stress σ_{02} increases from 590 to 1000 MPa. With growing σ_{02}, the concentration of the trapped hydrogen also increases considerably (from 35 to 54 ppm) (Figure 1). Data in Figure 2 shows that the loss of plasticity increases almost linearly with growing pre-strain. It can be seen that ε^H_{LOSS} for hydrogen charged samples is considerably higher than ε_{LOSS} for hydrogen uncharged samples.

With loss of plasticity of the hydrogen charged samples, the fracture mechanism changes from pit fracture at $\varepsilon = 0$ to quasi-cleavage mechanism at $\varepsilon = 20\%$. It should be noted that the correlation between σ_{02} and some parameters of SCC testing in NACE solution 13% Cr and high-strength low-alloy steels is discussed in [20].

It is shown that hydrogen microcracks in low-strained samples (0−5%) are formed primarily in ferrite grains, while in microcracks in high-strained samples (10−20%) occur in austenite grains.

5. Stress corrosion cracking mechanisms

There are several micromechanisms of SCC-induced brittle crack propagation [21]. One of them is hydrogen-enhanced decohesion approach (HEDE), and the other is associated with hydrogen-enhanced localized plasticity (HELP).

The former is based on the hypothesis that the introduced hydrogen reduces cohesive strength due to atomic lattice expansion and, consequently, to fracture energy reduction. This means that H reduces the energy barrier for decohesion either at the grain boundary or at the cleavage plane. And it is assumed that fracture starts in the maximum hydrostatic stress region σ_m at some distance from the tip of the initial crack. Hydrostatic stress is the main force for H diffusion from the material towards the tip of the crack. Diffusing H is accumulated in trap centers and causes lattice dilatation. Trap sites capability of holding H atoms is associated with binding energy and hydrogen diffusion activation energy. It is assumed that dislocations, grain boundaries, phase bound-

aries, inclusions and precipitates formed during thermomechanical treatment are the trap. In DSS, low diffusion activation energy in ferrite ($E_g = 12.5$ kJ/mol) defines high diffusion rate and low solubility H. For austenite, $E_g = 42$ kJ/mol defines low diffusion rate and, thus, high solubility H in austenite due to close-packed atoms in the FCC lattice.

Another mechanism [22,23] is associated with hydrogen-enhanced localized plasticity. Atomic hydrogen particles absorbed on the crack surfaces diffuse into a region in front of the crack tip in the FCC lattice and occupy octahedral interstitial. The presence of hydrogen in the lattice reduces the shear modulus and, therefore, the yield stress.

It is shown that two parallel dislocations with the same Burgers vectors in the FCC lattice will be pulled together creating a higher dislocation density in the sliding plane. Brittle crack initiation in the HELP mechanism occurs due to the shear decohesion along the sliding plane. This mechanism acting at the sharp notch or crack is confirmed by the increasing dislocation density at the grain boundary in austenite stainless steel when gaseous hydrogen is introduced [24]. It should be noted that the stress field near the crack tip will facilitate secondary crack initiation in the maximum shear stress point at the barrier and subsequent microcrack propagation towards the tip of the macrocrack in the embrittlement mode due to high dislocation density between the barrier and the crack tip. In addition, this stress field will activate the sliding systems of the adjacent grains and, as a consequence, the crack will move in zigzag fashion in the austenite phase. It should be noted that according to [21], the crack will propagate in the austenite phase only if this phase is weakened by hydrogen before austenite deformation. Otherwise, the austenite phase acts as a barrier for crack propagation. For example, in this case a crack in duplex steel will propagate along the phase interface between the austenite and ferrite.

In [25], the examination of microcracking areas near a U-shape notch in DSS samples subjected to cathodic hydrogen charging at 100 A/m^2 and external tensile stress $\sigma = 0.9\sigma_{02}$ reported a case of crack initiation in austenite grains, if their size was considerably lower than the average size in for the sample.

It is also pointed out in [25] that the external stress enhances hydrogen diffusion and increases hydrogen concentration near the crack tip. The maximum hydrogen concentration is achieved in the maximum hydrostatic stress area σ_m. It is also suggested that hydrogen reduces the critical crack initiation stress, because there is no cracking without hydrogen at the same σ value. Stress application also accelerates surface crack initiation.

6. Hydrogen impact on duplex steel embrittlement

Finally, the correlation between hydrogen concentration and duplex steel embrittlement will be discussed.

Much of the literature correlate hydrogen embrittlement with hydrogen concentration in duplex steel [26]. This assumption was checked in [27]. For tensile test, the authors used the slow strain rate testing (SSRT) method in various solutions. First, the samples were subjected to cathodic hydrogen charging at a current density of 200 A/m^2 during two weeks without deformation. Then, deformation was initiated and cathodic charging was continued to failure: hydrogen concentration was measured immediately after the failure. Additional tensile testing was carried out in air on uncharged samples. Hydrogen concentration in the broken samples was from 13 ppm(w) to 250 ppm(w). According to the authors, ferrite or phase boundaries could be the hydrogen trap sites.

The degree of sample embrittlement (embrittlement index) was defined by $t_{f,H}/t_{f,air}$ or by reduction of the broken sample cross-section RA_H/RA_{air}, where letters H and air denote the samples broken with and without hydrogen (t_f is time to failure).

It is shown that hydrogen embrittlement rate is highly dependent on the absorbed hydrogen concentration. Linear correlation between the embrittlement index logarithm and total hydrogen concentration logarithm was derived:

$$t_{f,H}/t_{f,air} = 0.032 \cdot C_H^{-0.34}, \quad (4)$$

$$RA_H/RA_{air} = 0.013 \cdot C_H^{-0.36}. \quad (5)$$

The extrapolation of the derived logarithmic dependence to the embrittlement index equal to one allowed to define the safe hydrogen concentration ($1 - 5ppm$) at which there is no loss of plasticity.

Conclusion

In view of the foregoing, the following conclusion may be made.

Most of cracks in DSS initiate and propagate in ferrite. When cracks come across austenite, they stop.

Phase boundaries in DSS act not only as powerful traps, but also make the diffusion paths more tortuous due to diffusion energy barrier at the interface.

Hydrogen diffusion and interaction with the traps are critical for understanding the hydrogen embrittlement resistance of steel.

Pitting corrosion resistance depends on the degree of nitrogen-doping of austenite and chromium-/molybdenum-doping of ferrite.

Plastic pre-strain reduces film plasticity and accelerates DSS dissolution.

Content of hydrogen-induced second phases and their hydrogen binding energy have considerable effect on the hydrogen embrittlement mechanism.

It is shown that hydrogen embrittlement rate is highly dependent on the absorbed hydrogen concentration. In some cases, correlation between the DSS embrittlement and yield stress is observed.

Conflict of interest

The authors declare that they have no conflict of interest.

References

[1] R. Silverstein, D. Eliezer. J. Alloys Comp., **720**, 451 (2017). DOI: 10.1016/j.jallcom.2017.05.286

[2] R. Silverstein, D. Eliezer. J. Alloys Comp., **644**, 280 (2015). DOI: 10.1016/j.jallcom.2015.04.176

[3] E. Barel, G. Ben Hamu, D. Eliezer, L. Wagner. J. Alloys Comp., **468** (1–2), 77 (2009). DOI: 10.1016/j.jallcom.2007.12.104

[4] R. Silverstein, D. Eliezer, B. Glain, D. Moreno. J. Alloys Comp., **648**, 601 (2015). DOI: 10.1016/j.jallcom.2015.07.029

[5] L. Claeys, I. De Graeve, T. Depover, K. Verbeken. Mater. Sci. Eng.: A, **797**, 140079 (2020). DOI: 10.1016/j.msea.2020.140079

[6] W. Wu, X. Zhang, W. Li, H. Fu, S. Liu, Y. Wang, J. Li. Corrosion Science, **202**, 110332 (2022). DOI: 10.1016/j.corsci.2022.110332

[7] E. Owczarek, T. Zakroczymski. Acta Mater., **48**, 3059 (2000). DOI: 10.1016/S1359-6454(00)00122-1

[8] R. Silverstein, D. Eliezer, E. Tal-Gutelmacher. J. Alloys Comp., **747**, 511 (2018). DOI: 10.1016/j.jallcom.2018.03.066

[9] R. Shi, Y. Ma, Z. Wang, X.-S. Yang, L. Qiao, X. Pang. Acta Mater., **200**, 686 (2020). DOI: 10.1016/j.actamat.2020.09.031

[10] D. Di Stefano, R. Nazarov, T. Hickel, J. Neugebauer, M. Mrovec, C. Elsässer. Phys. Rev. B, **93**, 184108 (2016). DOI: 10.1103/PhysRevB.93.184108

[11] T. Bellezze, G. Giuliani, G. Roventi, R. Fratesi, F. Andreatta, L. Fedrizzi. Mater. Corrosion, **67** (8), 831 (2016). DOI: 10.1002/maco.201508708

[12] Wen-Ta Tsai, Jhen-Rong Chen. Corrosion Science, **49** (9), 3659 (2007). DOI: 10.1016/j.corsci.2007.03.035

[13] C. Mendibide, C. Dessolin. Corrosion, **79** (2), 174 (2023). DOI: 10.5006/4225

[14] A.A. EL-Yazgi, D. Hardie. Corrosion Science, **40** (6), 909 (1998). DOI: 10.1016/S0010-938X(98)00022-5

[15] N. Sridhar, J. Kolts. Corrosion, **43** (11), 646 (1987). DOI: 10.5006/1.3583843

[16] T. Bellezze, G. Giuliani, A. Vicere, G. Roventi. Corrosion Science, **130**, 113 (2018). DOI: 10.1016/j.corsci.2017.10.012

[17] J. Yang, Q. Wang, K. Guan. Intern. J. Pressure Vessels and Piping, **110**, 72 (2013). DOI: 10.1016/j.ijpvp.2013.04.025

[18] R. Dakhlaoui, A. Baczmański, C. Braham, S. Wroński, K. Wierzbanowski, E.C. Oliver. Acta Mater., **54** (19), 5027 (2006). DOI: 10.1016/j.actamat.2006.06.035

[19] P. Tao, F. Ye, W. Cen, J. Zhao, Y. Wang, J. Gong. Results in Physics, **16**, 102820 (2020). DOI: 10.1016/j.rinp.2019.102820

[20] A.I. Petrov, M.V. Razuvaeva. ZhTF, **92** (10), 1588 (2022). (in Russian). DOI: 10.21883/JTF.2022.10.53251.154-22 [A.I. Petrov, M.V. Razuvaeva. Tech. Phys., **67** (10), 1366 (2020). DOI: 10.21883/TP.2022.10.54364.154-22]

[21] V. Olden, C. Thaulow, R. Johnsen. Mater. Designe, **29**, 1934 (2008). DOI: 10.1016/j.matdes.2008.04.026

[22] P. Sofronis, Y. Liang, N. Aravas. Europ. J. Mechanics–A/Solids, **20** (6), 857 (2001). DOI: 10.1016/S0997-7538(01)01179-2

[23] M.L. Martin, M. Dadfarnia, A. Nagao, S. Wang, P. Sofronis. Acta Mater., **165**, 734 (2019). DOI: 10.1016/j.actamat.2018.12.014

[24] D.P. Abraham, C.J. Altstetter. Metall. Mater. Trans. A, **26**, 2849 (1995). DOI: 10.1007/BF02669643

[25] P. Tao, J. Gong, Y. Wang, W. Cen, J. Zhao. Intern. J. Pressure Vessels and Piping, **180**, 104031 (2020). DOI: 10.1016/j.ijpvp.2019.104031

[26] F. Iacoviello, M. Habashi, M. Cavallin. Mater. Sci. Eng.: A, **224**, 116 (1997). DOI: 10.1016/S0921-5093(96)10545-1

[27] T. Zakroczymski, A. Glowacka, W. Swiatnicki, Corrosion Science, **47**, 1403 (2005). DOI: 10.1016/j.corsci.2004.07.036

Translated by Ego Translating